Electrochemistry at Chemically Assembled Single-Wall Carbon Nanotube Arrays

ARTICLE *in* THE JOURNAL OF PHYSICAL CHEMISTRY B · DECEMBER 2005

Impact Factor: 3.3 · DOI: 10.1021/jp052666r · Source: PubMed

Electrochemistry at Chemically Assembled Single-Wall Carbon Nanotube Arrays

Peng Diao[†,‡] and Zhongfan Liu*[,†]

Center for Nanoscale Science & Technology, College of Chemistry & Molecular Engineering, Peking University, Beijing 100871, People's Republic of China, and School of Materials Science and Engineering, Beijing University of Aeronautics and Astronautics, Beijing 100083, People's Republic of China

Received: May 21, 2005; In Final Form: August 31, 2005

Single-wall carbon nanotubes (SWNTs) chemically assembled on gold substrates were employed as electrodes to investigate the charge transfer process between SWNTs and the underlying substrates. Cyclic voltammetry (CV) indicates that the assembled SWNTs allow electron communication between a gold electrode and the redox couple in solution, though the SWNTs are linked directly onto the insulating monolayer of 11-amino-*n*-undecanethiol (AUT) on the Au substrate. An electron transfer (ET) mechanism, which contains an electron tunneling process across the AUT monolayer, is proposed to explain the CV behavior of Au/AUT/SWNT electrodes. Electrochemical measurements show that the apparent electron tunneling resistance, which depends on the surface density of assembled SWNTs, has apparent effects similar to those of solution resistance on CV behavior . The theory of solution resistance is used to describe the apparent tunneling resistance. The experimental results of the dependence of ET parameter ψ on the potential scan rate v are in good agreement with the theoretical predictions. Kinetic studies of the chemical assembly of SWNTs by atomic force microscopic (AFM), electrochemical, and Raman spectroscopic methods reveal that two distinct assembly kinetics exist: a relatively fast step that is dominated by the surface reaction, and a successive slow step that is governed by bundle formation.

1. Introduction

Since the discovery of single-wall carbon nanotubes (SWNTs) in 1993,[1] these molecular-scale wires have been of great interest because of their unique structure, high mechanical strength, chirality-dependent conductivity, and good chemical stability. These properties make carbon nanotubes (CNTs) good candidates for nanoelectronic devices,[2] electron field emission sources,[3] scanning probes,[4] actuators,[5] and chemical sensors.[6] Many potential applications of CNTs require length-controlled and well-aligned CNTs. However, CNTs are usually long and highly tangled. Several groups have succeeded in fabricating highly oriented carbon nanotubes by using a chemical vapor deposition method,[3b,7] but this method is successful only for multiwall carbon nanotubes. Recently, we[8] and others[9−11] have separately developed wet chemical approaches to immobilization of SWNTs onto solid surfaces. These approaches were also successful to prepare well-aligned short SWNT arrays,[8a−c,f,9−11] and thus allow further studies using these ordered SWNT systems. In our previous work, we demonstrated that aligned SWNTs act as nanoelectrodes that can exchange electrons between a conductive substrate and a redox couple in solution.[8c] Gooding et al.[10] and Willner and co-workers[11a] showed that SWNTs immobilized on a gold electrode can be employed as nanowires that allow electron communication between the underlying electrode and electroactive proteins chemically bonded on SWNTs. Furthermore, Willner and co-workers[11b] also demonstrated that well-aligned SWNTs, which bridge the CdS nanoparticles and the gold electrode, greatly enhance the photoconversion efficiency. These studies imply that aligned-SWNT arrays have great potentials for electrochemical sensors, bioelectronic devices, and solar cells.

The preparation strategy for aligned SWNT arrays is to covalently or electrostatically immobilize one end of preshortened SWNTs on solid surfaces,[8−11] as shown in Figure 1a. Since all the above-mentioned applications of aligned SWNT arrays involve electron transfer (ET) between the underlying substrate and redox centers, which may be either attached to the external surface of SWNT or freely diffusing in the contact electrolyte, it is necessary to clarify the entire ET process. As shown in Figure 1b, ET in the aligned SWNT system includes three steps: (1) ET between redox centers and SWNTs, (2) electron transportation within SWNTs, and (3) ET between SWNTs and the underlying electrodes. The first step is well understood because it has ET characteristics similar to those between redox centers and carbon electrodes. For the second step, SWNTs were shown to be efficient conductive nanowires.[11] As to the third step, however, no work has been reported even through the third step is very important to understand the whole ET mechanism in the above-mentioned systems, since there is an insulating organic monolayer between SWNTs and substrates.

Electrochemistry is one of the effective techniques to study ET between substrates and electroactive or conductive species immobilized on the substrates. In this work, we use electrochemical means as the main techniques to study the ET process at chemically assembled SWNT electrodes. An ET model based on electron tunneling between the substrate and the tethered carbon nanotubes is proposed to explain the electrochemical behavior. Moreover, kinetic studies of the assembly process of SWNTs are performed by AFM, electrochemical, and Raman spectroscopic methods.

* Corresponding author: tel & fax 86-10-6275-7157; e-mail zfliu@pku.edu.cn.
† Peking University.
‡ Beijing University of Aeronautics and Astronautics.

10.1021/jp052666r CCC: $30.25
Published on Web 10/14/2005

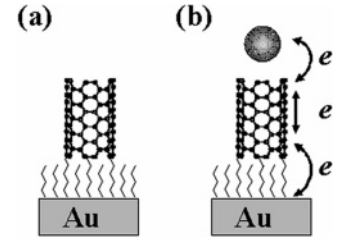

Figure 1. (a) Strategy for preparing aligned SWNT arrays. (b) Charge transfer in the aligned SWNT system.

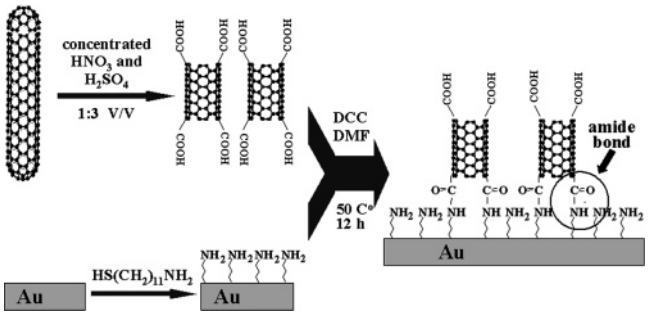

Figure 2. Schematic representation of the formation of SWNT assemblies.

2. Experimental Section

Chemicals. The 11-amino-*n*-undecanethiol (AUT) was purchased from Dojindo Co. $Ru(NH_3)_6Cl_3$ was obtained from Alfa Aesar (A. Johnson Matthey Co.). Both were of analytical grade and used as received. Other chemicals were of analytical grade. The AUT solution was prepared by dissolving AUT in absolute ethanol and its final concentration was 1 mM.

Preparation of AUT Monolayer on Gold. Gold substrates were prepared on Si wafers by sputtering with 150 nm Au (99.99%). A 10 nm Cr layer was deposited prior to Au deposition to improve adhesion to the Si wafer. Prior to use, the gold substrates were cleaned in Piranha solution (1:3 mixture of 30% H_2O_2/concentrated H_2SO_4, v/v) at 90 °C for 10 min followed by rinsing with copious water and absolute ethanol, successively. AUT monolayers were formed by immersing gold substrates in 1 mM AUT solution for 24 h. Prior to surface condensation with carboxylic acid groups at SWNT ends, the monolayer-coated gold substrates were washed with ethanol to rinse off residual AUT molecules and then dried in a stream of high-purity N_2.

Preparation of Chemically Assembled SWNTs. The SWNTs used in this work were synthesized by the chemical vapor deposition method with Fe−Mo catalyst.[12] Transmission electron microscopy shows the typical diameters of as-prepared SWNTs are 1.1∼1.3 nm. The purification and chemical shortening of long SWNTs followed the same procedure described elsewhere.[8a] The fuctionalization of SWNTs with carboxylic acid groups was accomplished in the process of chemical shortening.[13] Figure 2 shows the strategy of preparing the Au/AUT/SWNT electrode. The -COOH groups at the end of shortened SWNTs were used to condense with $-NH_2$ groups on the top of the AUT monolayer.[8a,c−f,10,11] The surface condensation reaction results in the formation of amide bonds that immobilize SWNTs on the Au surface. The procedure of surface condensation reaction were described elsewhere.[8c−e] In detail, the shortened SWNTs were first dispersed in *N*,*N*-dimethylformamide (DMF) to give a ca. 0.2 mg/mL black solution. Dicyclohexylcarbodiimide (DCC) was used as condensing agent; its concentration in the SWNT solution was ca. 0.5 mg/mL. The surface condensation was then carried out by immersing the AUT-coated gold substrate in SWNT solution at 50 °C for required time. Before electrochemical, AFM, and Raman measurements, the SWNT-modified substrates were exposed to ultrasonic briefly in absolute ethanol to get rid of the SWNTs physically adsorbed on AUT monolayers. Then, the resulting samples were rinsed with absolute ethanol and dried with high-purity N_2.

Electrochemical Measurements. Cyclic voltammetry measurements were performed on a CHI660A electrochemical workstation (CH Instruments Co.). The exposed area of working electrode is 0.26 cm^2. All CV experiments were carried out in a conventional three-electrode cell at 17 ± 1 °C. A saturated calomel electrode (SCE) and a Pt wire were employed as reference and counter electrodes, respectively. All potentials are reported with respect to SCE.

Atomic Force Microscopic Measurements. AFM characterizations were performed in the tapping mode in air with a Nanoscope IIIa microscopy (Digital Instruments).

Raman Measurements. Polarized Raman spectra were recorded at the cross section of the sample on a Renishow Raman imaging system 1000 equipped with a He−Ne laser from Spectra Physics (model 127-25RP, $\lambda_0 = 632.8$ nm) and a Peltier-cooled charge-coupled device (CCD) detector. A 50× objective mounted on an Olympus BH-2 microscope was used to focus the laser beam into a spot approximately 1 μm in diameter and to collect the backscattered spectra of the samples. A half-wave plate was inserted before the objective of the microscope to ensure that the polarization of the incident light is perpendicular to the substrate (parallel to the SWNT axis).

3. Results and Discussion

Electrochemical Behavior of Au/AUT/SWNT Electrode. In our previous works, we demonstrated, by AFM and polarized Raman spectrum, that most SWNTs with lengths of ca. 20∼100 nm were immobilized on Au substrates with only one end tethered to the AUT monolayers,[8c] while for the relatively "long" SWNTs (>300 nm), AFM results reveal that SWNTs are more likely to lie sideways on the gold surface. These results were further confirmed by two other groups.[10,11] We also showed by Fourier transform infrared spectroscopy that SWNTs were immobilized on the gold surface via amide bonds.[8c]

Herein, the as-prepared SWNT alignments were employed as electrodes to investigate the ET process between SWNTs and the underlying substrates. The CV plots of Au/AUT/SWNT electrodes in supporting electrolyte solution (1 M KCl) (not shown) show only double-layer charging currents, revealing that the SWNTs are electrochemically inactive within the potential window applied (−0.5∼0.1V). Figure 3 shows the cyclic voltammograms of bare Au, Au/AUT, and Au/AUT/SWNT electrodes in $Ru(NH_3)_6Cl_3$ solution. The peak separation of 60 mV at the bare gold electrode reflects the reversibility of $Ru(NH_3)_6^{3+/2+}$ as an outer-sphere redox couple (Figure 3a). As shown in Figure 3b, the absence of redox current peaks at the Au/AUT electrode indicates that the AUT monolayer greatly inhibits the heterogeneous ET between Au substrate and redox species in solution. However, when SWNTs were covalently linked to AUT monolayer, the redox peaks reappeared, as if the hydrocarbon chain of AUT became conductive (Figure 3c). This CV behavior is quite similar to that of gold nanoparticle monolayers formed on conducting substrate via insulating organic film.[14] To rule out the possibility that AUT molecules desorbed in DMF and formed pinholes during the attachment of SWNTs, we ran a blank experiment in which the Au/AUT

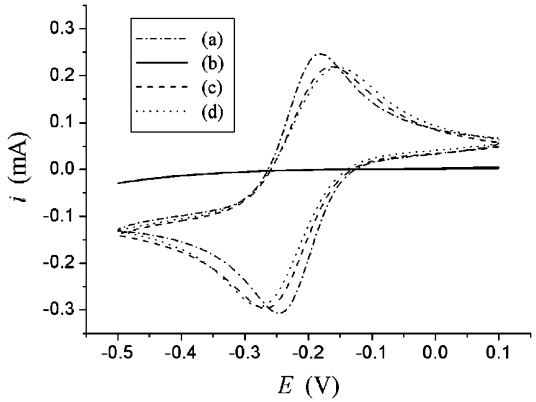

Figure 3. Cyclic voltammograms of (a) bare Au, (b) Au/AUT, (c) Au/AUT/SWNTs, and (d) Au/AUT/SWNTs after reimmersion in AUT solution for 12 h. The electrolyte is 5 mM $Ru(NH_3)_6Cl_3$ in 1 M KCl. Scan rate was 100 $mV \cdot s^{-1}$.

electrode was immersed in DMF containing DCC, but without SWNTs, for 12 h at 50 °C. The CV feature of as-treated Au/AUT electrode is almost identical to that of untreated Au/AUT, suggesting that no detectable pinholes were generated from the AUT desorption. Before ascribing the return of redox peaks to the presence of SWNTs, we need to remove another ambiguity, which is whether the attachment of SWNTs might disturb the AUT monolayer and therefore lead to local defects in the organic films, allowing access of the electroactive ions. In fact, this possibility is a common issue for both SWNTs and nanoparticle assemblies covalently immobilized on a conductive surface via insulating organic film.[14] So, whether there are large number of nanoparticle- or SWNT-induced local defects in the linking organic layer should be addressed before these systems are used in fundamental research and applications, especially in the field of electrochemistry.

For the gold nanoparticle assembly system, this issue is difficult to study because repairing the organic film with corresponding molecules may lead to coating of the gold nanoparticles that then distorts the redox waves. For this reason, no work has been reported, to our knowledge, to explore whether there are some nanoparticle-induced local defects that might affect the electrochemical behavior of gold nanoparticle assemblies. As for the Au/AUT/SWNT electrode, the small interaction between SWNT side walls and AUT molecules makes it possible to repair the SWNT-induced monolayer defects, if there are any, without affecting the electrochemical behavior of SWNTs. So, we believe Au/AUT/SWNT is a good model system to elucidate the above-mentioned issue. The following experiments are designed to study this issue.

The newly prepared Au/AUT/SWNT electrodes were reimmersed in AUT solution for 12 h. Then the resulting SWNT assemblies were used in CV experiments to see if the redox waves disappeared or decreased. The result is shown in Figure 3d. As discussed above, AUT will not affect the electrochemical features of SWNTs because it cannot absorb on the side walls or ends of SWNTs due to the weak interaction between them. On the other hand, during the readsorption procedure, the strong interaction between sulfur and gold, the hydrogen bonds between $-NH_2$ groups, as well as the van der Waals' force between alkyl chains, will result in the insertion of AUT molecules into the local defects that were supposed to be induced by the attachment of SWNTs. Therefore, if there are large numbers of SWNT-induced defects and these defects dominate the redox current of Au/AUT/ SWNTs, we should observe that the redox waves decrease greatly after reimmersion in AUT solution. By

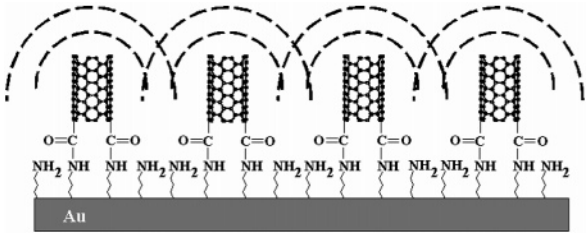

Figure 4. Schematic representation of the diffusion behavior of SWNT assembly electrode.

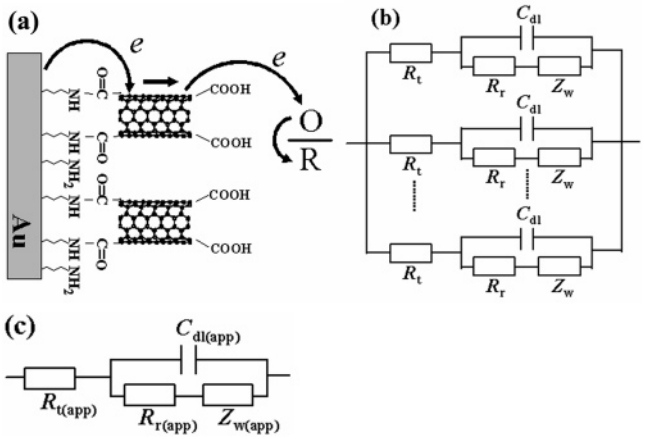

Figure 5. (a) Schematic representation of electron-transfer process at an assembled SWNT electrode. (b) Corresponding equivalent circuit. (c) Simplified equivalent circuit when it is assumed that all corresponding elements are the same in value.

comparison of Figure 3 panels d and c, it is obvious that the cyclic voltammogram of as-treated Au/AUT/SWNTs was almost the same as that of untreated sample, indicating that the attachment of SWNTs induces no or undetectable local defects on the AUT monolayer. In other words, the presence of SWNTs, which serve as "electron transfer stations" in the ET process, is the only cause of the turn-on of the charge transportation between gold substrate and redox couples in solution. We believe this result also provides some insight into the ET process of gold nanoparticle assemblies.

There is another issue that needs to be pointed out. In our CV experiments, we found that the peak current of Au/AUT/SWNTs never exceeds that of bare Au, although the specific area of electrode is greatly increased after linkage of SWNTs. We believe this is due to the similar diffusion characteristics of Au/AUT/SWNTs to those of closely packed microelectrode arrays.[15] As we know, when the diffusion of the redox couple is the rate-determining step, the electrode area obtained by cyclic voltammetry and other electrochemical methods actually reflects the area of the diffusion layer. For a smooth electrode, the area of diffusion layer is the same as that of the electrode. For a rough electrode, however, the area of diffusion layer is not definitely the same as the real surface area of the electrode. There are two different cases: (1) If the size of protrusions (or pits) and the distance between them are in the same range as or larger than the thickness of diffusion layer (for aqueous solutions, a typical diffusion layer thickness of ca. 10^{-4} cm is built up in 1 ms, 10^{-3} cm in 0.1 s, and 10^{-2} cm in 10 s),[16] the measured area reflects the real surface area of the rough electrode. (2) However, if the size of protrusions (or pits) and the distance between them are much smaller than the diffusion layer thickness, the diffusion layers produced by individual protrusions will overlap and finally form a uniform layer, which has the same diffusion area as that of a smooth electrode. Under

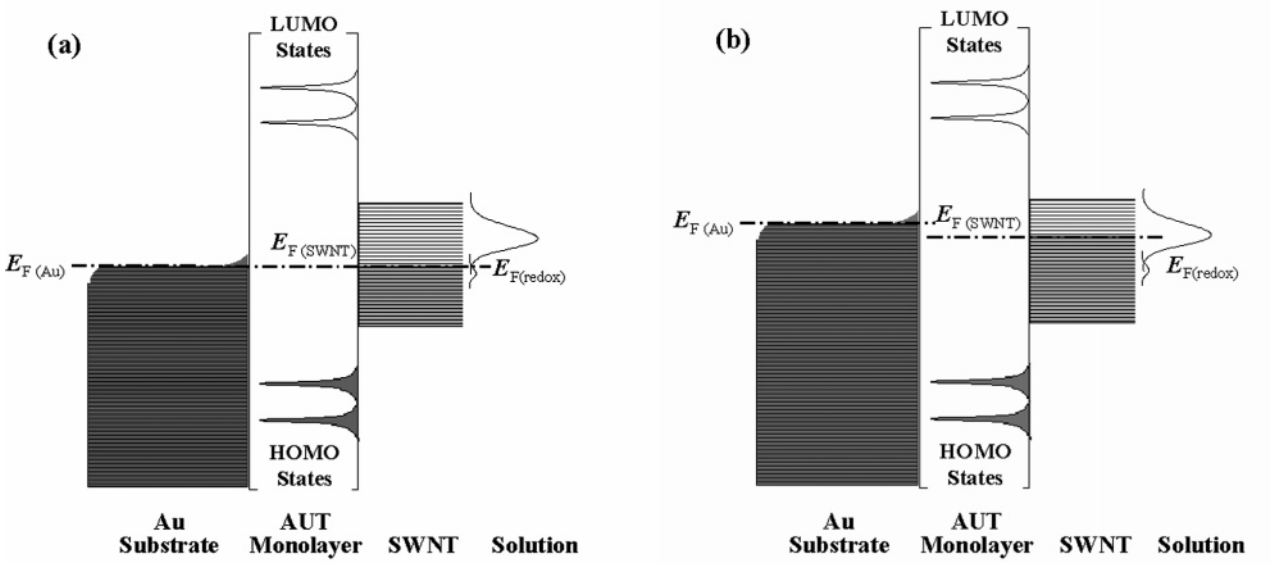

Figure 6. Density of electronic states distribution diagram for a single assembled metallic SWNT electrode in contact with solution containing reducible electroactive species: (a) in equilibrium; (b) in cathodic process. The filled electronic states are shaded.

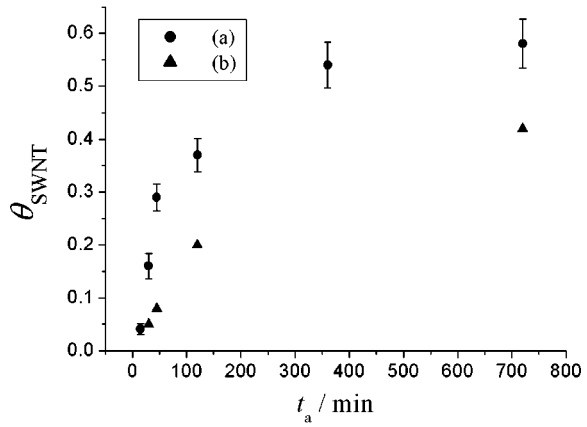

Figure 7. Dependence of surface coverage of SWNTs on assembly time obtained by (a) AFM and (b) electrochemical methods.

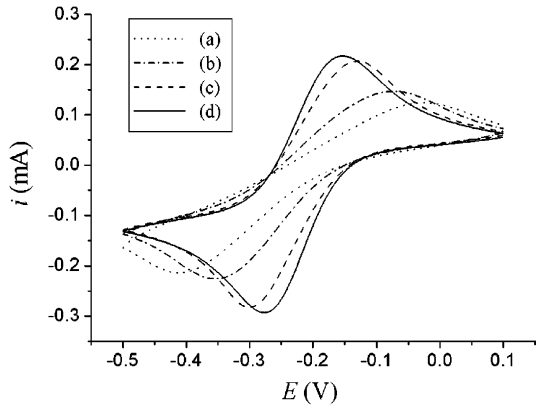

Figure 8. Cyclic voltammograms of Au/AUT/SWNT electrodes with different assembly times: (a) 30 min, (b) 45 min, (c) 2 h, and (d) 12 h. The electrolyte is 5 mM $Ru(NH_3)_6Cl_3$ in 1 M KCl. Scan rate was 100 $mV \cdot s^{-1}$.

this condition, the area measured by electrochemical methods will be the same as the projected area (geometric area) of the rough electrode. For Au/AUT/SWNT electrodes, the size of aligned SWNTs and the distances between them are much smaller compared to the diffusion layer thickness (10^{-3}—10^{-2} cm) built in the experimental duration. Therefore, as shown in Figure 4, the diffusion layers generated by nearby SWNTs will overlap and finally produce one uniform diffusion layer, which has the same geometric area as that of the underlying gold electrode.

Electron-Transfer Mechanism. Because SWNTs are tethered directly to the AUT monolayers, there must be an electron tunneling process between Au substrates and SWNTs due to the insulating nature of the AUT monolayer. We believe the SWNTs serve as Coulombic islands (electron transfer stations), which are necessary to funnel electrons between the conducting substrate and the remote redox centers in solution. The whole charge transfer at an Au/AUT/SWNT electrode is schematically represented in Figure 5a, wherein the ET consists of three steps (taking the cathodic process for example): (1) electron tunneling from gold to SWNTs, (2) electron transportation within SWNTs, and (3) heterogeneous ET from SWNT ends or sidewalls to $Ru(NH_3)_6^{3+}$.[17] Although some defects, which were induced to the sidewalls of SWNTs during the shortening procedure, may break, to some extent, the large p-conjugation system within SWNT and generate local traps for charge transport, it has been shown that the conductivity of the immobilized SWNTs is good enough to make SWNTs act as nanowires.[11] Moreover, facile heterogeneous ET kinetics was reported between $Ru(NH_3)_6^{3+/2+}$ and carbon electrodes,[18] such as carbon nanotube.[17] Therefore, the second and third steps in ET can be well understood.

The first step in the whole ET process is, in fact, the key step to understand the electrochemical behavior of Au/AUT/SWNTs in electrolyte containing redox species. The energy diagram for the ET process at an individual metallic SWNT nanoelectrode is shown in Figure 6. At equilibrium, the Fermi levels of Au [$E_{F(Au)}$], SWNT [$E_{F(SWNT)}$], and the redox couple $Ru(NH_3)_6^{3+}$ are in the same position (see Figure 6a). With the negative scan from equilibrium potential, $E_{F(Au)}$ is increased and exceeds $E_{F(SWNT)}$. As a result, electrons are injected into the unoccupied states of SWNTs via tunneling to make the Fermi levels of SWNT equal to that of Au, as shown schematically in Figure 6b. The increased $E_{F(SWNT)}$ significantly enhanced electron-transfer probability from SWNT to the oxidized species of the redox couple [$Ru(NH_3)_6^{3+}$], and in the meantime greatly reduced the possibility of electron transfer from $Ru(NH_3)_6^{2+}$ to SWNTs, resulting in a great increase of reduction current in the CV plot. In a positive scan, $E_{F(SWNT)}$ decreases with $E_{F(Au)}$,

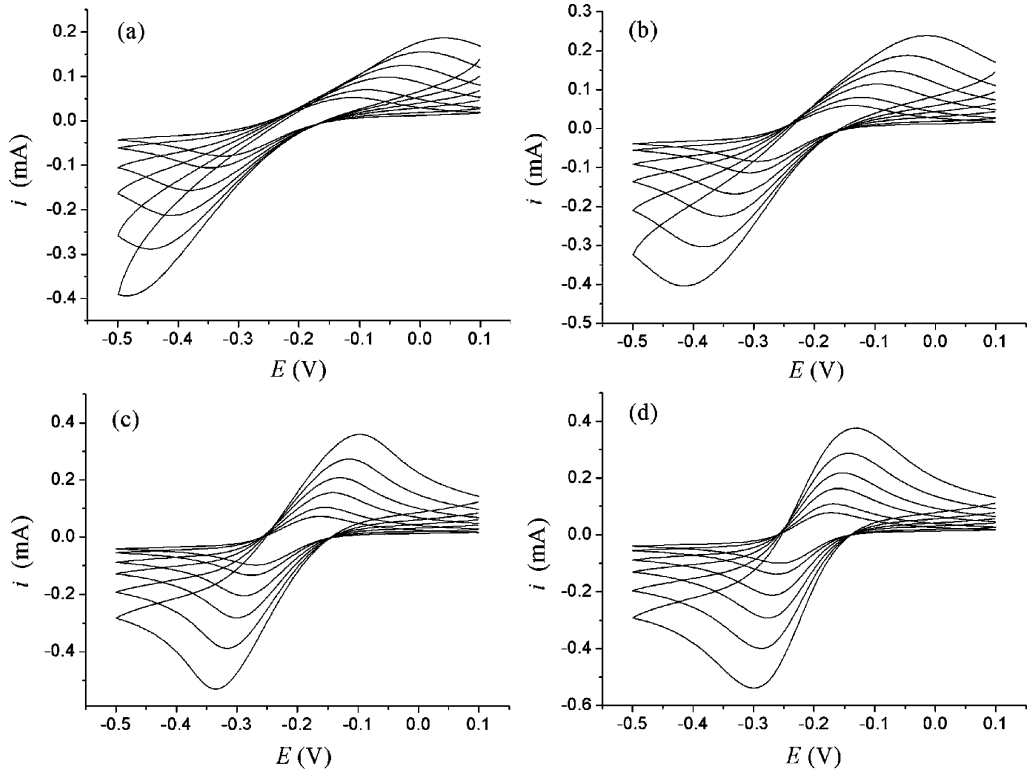

Figure 9. Influence of scan rate on CV behavior of Au/AUT/SWNTs prepared with different assembly times: (a) 30 min, (b) 45 min, (c) 2 h, and (d) 12 h. The electrolyte is 5 mM $Ru(NH_3)_6Cl_3$ in 1 M KCl. Scan rates were 10, 20, 50, 100, 200, and 400 $mV \cdot s^{-1}$.

and when $E_{F(Au)}$ is lower than the equilibrium potential, reversed electron transfer occurs.

From the CV behavior of Au/AUT electrode (Figure 3b) we note that, within the potential window applied, electron transfer between metal substrate and redox species in electrolyte is almost totally hindered by the AUT monolayer, suggesting that electron tunneling via AUT monolayer is difficult to take place. This is in accordance with CV behaviors of gold electrodes coated with long-chain self-assembled monolayers.[19] Then there rises an important question: why ET between a gold electrode and a redox couple in the presence of SWNTs becomes much easier compared to that in absence of SWNTs. We believe this is due to the following reasons. For Au/AUT/SWNTs, the large p-conjugated system within SWNT makes itself both an electron acceptor and a donor. In a cathodic process, SWNTs accept electrons from gold and the extra charge will increase the energy level of SWNTs and then make SWNTs donate electrons to the redox couple either in solution or covalently linked to SWNTs. In an anodic process, SWNTs donate electrons to the gold electrode, and in the meantime accept electrons from the redox couple. The large number of occupied and unoccupied states within SWNT allows not only facile ET between SWNTs and redox couples but also efficient electron tunneling between SWNTs and the underlying substrate. This means that the immobilized SWNTs serve as tiny electron relay stations that mediate electrons between the metal electrode and redox centers. However, for the Au/AUT system, there are no such "electron-active" sites on the AUT monolayer to accept and donate electrons. The only way for ET, is for electrons to tunnel across the AUT monolayer, from gold substrate to the unoccupied states of oxidized species in a cathodic process and from filled states of reduced species to gold electrode in an anodic process.

In addition, the form of electron tunneling is different for Au/AUT/SWNT and Au/AUT electrodes. ET between metal substrate and SWNTs is quite similar to that between gold and redox centers that are attached to the gold surface by a self-assembled monolayer (SAM), since both systems have similar structures in which insulating SAMs were covalently sandwiched between electrode and electron acceptors or donors. It has been shown that through-bond tunneling is the ET mechanism in the system of Au/SAM/redox centers.[20] CV experiments demonstrated that the efficiency of through-bond tunneling is high enough that reversible CV plots can be obtained,[20−22] implying that redox centers can rapidly exchange electrons with the underlying electrode via tunneling. Therefore, it is reasonable to believe that the efficient through-bond tunneling occurs between SWNTs and gold at Au/AUT/ SWNT electrodes. As to Au/AUT electrodes, there are no chemical bonds directly linking the redox centers and the electrodes; thus through-space tunneling is the only possible ET mechanism. If electron tunneling across insulating barriers is involved in ET, the redox current at any potential should decreases exponentially with increasing distance:

$$i = i_0 \exp(-\beta d) \tag{1}$$

where i_0 is the current measured at a bare electrode, d is the thickness of the barrier, and β is the electron tunneling coefficient. The β value for through-bond tunneling was obtained to be 1.06 per methylene group,[20] which corresponds to 0.85 $Å^{-1}$ (1.25 Å/methylene group).[23] This β value is much smaller than that of 1.3−1.8 $Å^{-1}$ estimated for through-space tunneling,[20] indicating that, in principle, through-bond tunneling is easier than through-space tunneling. Moreover, single molecular conductivity measurements by AFM demonstrated that the tunneling efficiency through alkanedithiols with both ends separately bonded to two gold electrodes is much higher than that through alkanethiols with only one end bonded to gold.[24,25] All this accounts for the high tunneling efficiency at Au/AUT/ SWNT electrode.

Effect of Assembly Time. The assembly time t_a has great influence on the surface density of SWNTs. The fractional

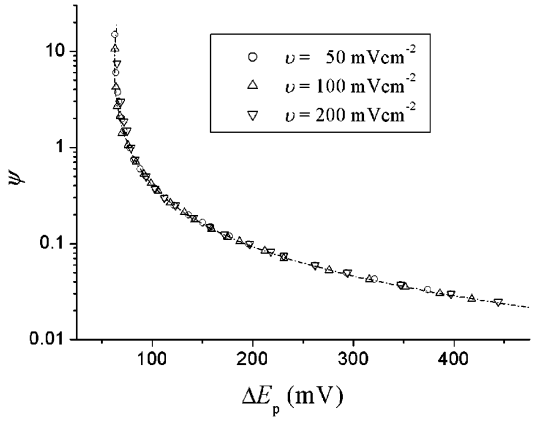

Figure 10. Running curve showing variation of ψ with peak potential separation ΔE_p.

surface coverage of SWNT can be estimated by AFM experiments.[10] From the average diameter and the surface density of the needlelike protrusions, which were obtained in AFM images,[8c] the fractional coverage of SWNT (θ_{SWNT}) at various assembly times t_a can be figured out and the results are shown in Figure 7a. The increase of θ_{SWNT} with increasing duration of the assembly step is generally consistent with previous works.[8a,10,11] The only difference is that the saturated θ_{SWNT} values in this work is ca. 0.59, which is nearly 50% higher than that obtained by Gooding et al.[10] using the same AFM method. The higher θ_{SWNT} value is ascribed to the long-chain linking monolayer used in this work. It has been shown that long chain alkanethiols form well-ordered, highly packed, stable, and pinhole-free SAMs. Moreover, as chain length decreases, SAM structure becomes disordered with lower packing density and coverage.[19,23] Therefore, compared to cysteamine (HSC_2NH_2) used in previous works,[8a,10,11] AUT ($HSC_{11}NH_2$) used in this work should form SAMs with higher ordering and packing density, and thus leads to higher surface coverage of SWNTs during modification.

Figure 8 shows the influence of assembly time on the electrochemical behavior of Au/AUT/ SWNT electrode. It can be clearly seen from Figure 8 that the redox peak separation decreases when the surface modification time is increased. As mentioned above, all works concerning aligned SWNT arrays have shown that the surface density of SWNTs increases with longer assembly time; the decrease of redox peak separation is believed to be related to the increase of SWNT density with surface modification time. The reason higher surface density of SWNTs leads to more reversible CV features will be discussed in detail later.

Electron tunneling can be characterized by tunneling resistance,[26] which is defined as the ratio of applied bias to tunneling current. The tunneling resistance, R_t, increases exponentially with separation according to[26a]

$$R_t = R_0 \exp(\beta d) \tag{2}$$

where R_0 is the effective contact resistance of the two separated phases and β and d have the same meanings as in eq 1. According to the ET process shown in Figure 5a, we use the equivalent circuit (EQC) that consists of a tunneling resistance R_t in series with a parallel double layer capacitance C_{dl}, a reaction resistance R_r, and a mass transfer impedance Z_w, to model the electrochemical process at an individual SWNT electrode (see one parallel branch of EQC in Figure 5b). The solution resistance is omitted here since it is much smaller than R_t when the concentration of supporting electrolyte is high (e.g., 1 M KCl). For the whole Au/AUT/SWNT electrode, ET at each SWNT occurs in parallel; thus we can use the EQC shown in Figure 5b to analyze the electrochemical process at the entire working electrode.

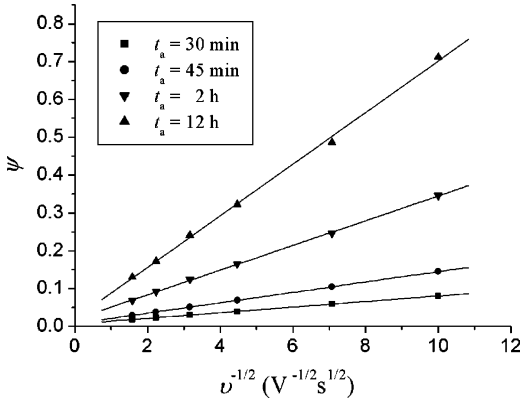

Figure 11. ψ vs $\upsilon^{-1/2}$ plots at different assembly times. ψ values at different scan rate are obtained by first measuring ΔE_p in Figure 9 and then finding the corresponding ψ in the running curve shown in Figure 10.

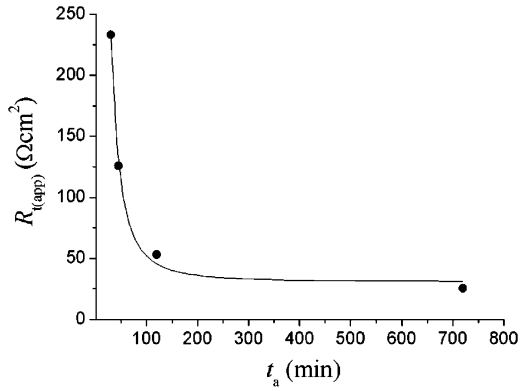

Figure 12. Dependence of normalized apparent electron tunneling resistance on assembly time.

If we assume that the values of the corresponding elements in Figure 5b are the same, the EQC for the entire Au/AUT/ SWNT electrode can be simplified to the one that contains an apparent electron tunneling resistance $R_{t(app)}$, in series with a parallel apparent capacitance $C_{dl(app)}$, an apparent reaction resistance $R_{r(app)}$, and a Warbug impedance $Z_{w(app)}$, as shown in Figure 5c. On the basis of the above assumption, the following equation can be obtained:

$$R_{t(app)} = R_t/n \tag{3}$$

Here n is the number of SWNTs immobilized on the Au substrate in one unit area (surface density of SWNTs). From eq 3, we know that $R_{t(app)}$ decreases with increasing density of SWNTs on Au surface. The simplified EQC is actually the same in form as that of a traditional macroelectrode. The only difference is that, in our case, the apparent electron tunneling resistance $R_{t(app)}$ replaces the solution resistance R_s. Because the ET between carbon electrode and $Ru(NH_3)_6^{3+/2+}$ is very fast,[17,18] the anodic and cathodic peak potential separation (ΔE_p) should be 60 mV if $R_{t(app)}$ is negligible. However, as shown in Figure 8, ΔE_p obtained at Au/AUT/ SWNT electrodes with various assembly times is much larger than 60 mV, indicating that the apparent effects of $R_{t(app)}$ on the CV behavior of Au/AUT/ SWNT electrode is similar to that of solution resistance R_s on the CV behavior of bare macroelectrode.[27] Moreover, the increase of ΔE_p with increasing scan rate (see Figure 9) also supports that $R_{t(app)}$ has similar effects on CV plots to R_s.[27]

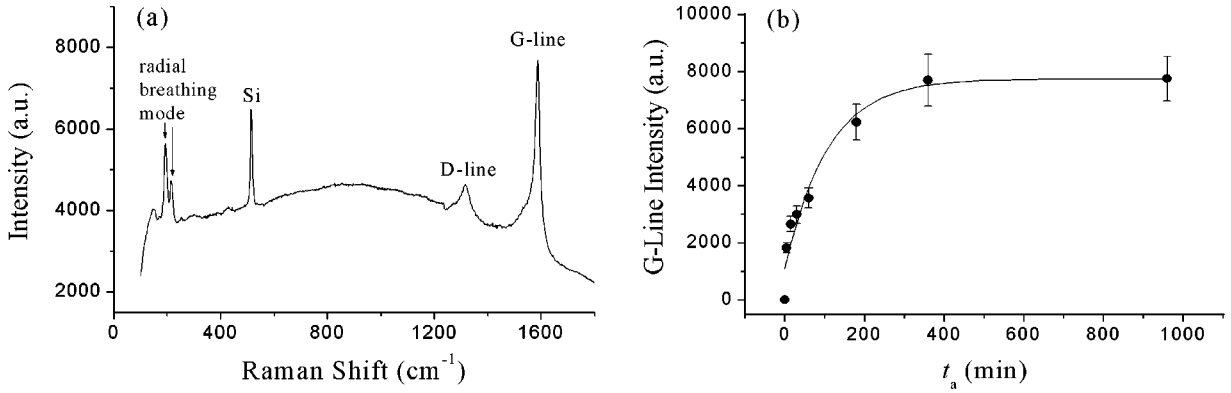

Figure 13. (a) Typical polarized Raman spectrum obtained at cross-section of Au/AUT/SWNT electrodes with assembly time of 6 h. (b) Dependence of G-line (sp^2 C−C stretching mode of SWNTs in polarized Raman spectrum) intensity of SWNTs on assembly time.

According to the above discussion, we use the theory of solution resistance to describe $R_{t(app)}$. The effect of R_s on CV behavior can be expressed as[27]

$$\psi = (RT)^{3/2}/[(nF)^{5/2}D_O{}^{1/2}\pi^{1/2}Av^{1/2}C_O{}^*R_s] \qquad (4)$$

where ψ is a charge-transfer parameter, A is the area of the electrode, v is the scan rate, and D_o and C^*_o are the diffusion coefficient and the concentration of oxidized species, respectively. Other parameters have their usual meanings. In our case, we replace R_s with $R_{t(app)}$ in eq 4 and obtain

$$\psi = (RT)^{3/2}/[(nF)^{5/2}D_O{}^{1/2}\pi^{1/2}Av^{1/2}C_O{}^*R_{t(app)}] \qquad (5)$$

ψ can be obtained experimentally from the peak potential separation ΔE_p. To obtain ψ at each ΔE_p, it is necessary to establish the $\psi \sim \Delta E_p$ relationship. In this work, the running curve of ψ vs ΔE_p was obtained at a bare Au electrode in $Ru(NH_3)_6^{3+/2+}$ solution with a resistance box inserted between the potentiostat and the working electrode. Part of the potentials applied to the working electrode will drop on the inserted resistance and made it play the role of solution resistance. By giving the inserted resistance, we obtained the ΔE_p values from CV plot. The corresponding ψ value can be calculated from eq 4 by use of R_s values given by the resistance box. Thus, the running curve of ψ vs ΔE_p was obtained, as illustrated in Figure 10. The running curves obtained at different scan rates are also shown in Figure 10. The coincidence of these curves indicates the reliability and stability of our electrochemical system.

According to eq 5, a straight line should be obtained at the Au/AUT/SWNT electrodes if ψ is plotted against $v^{-1/2}$, and then $R_{t(app)}$ can be calculated from the slope of the line. Figure 11 shows the ψ versus $v^{-1/2}$ plot of Au/AUT/SWNTs with different assembly times t_a. In Figure 11, ψ values at different scan rates are determined by first measuring ΔE_p in Figure 9 and then finding the corresponding ψ value in the running curve shown in Figure 10. Two features are worth noticing in Figure 11. First, straight lines are obtained at different t_a, indicating good agreement of experimental results with theoretical predictions. Second, the slope of the line increases monotonically with increasing t_a, suggesting that $R_{t(app)}$ decreases when t_a is increased. On the basis of eq 3, this means the surface density of SWNTs increases with longer assembly time.

Kinetics of the Chemical Assembly of SWNTs. Since $R_{t(app)}$ is dominated by the surface density of assembled SWNTs (eq 3), the dependence of $R_{t(app)}$ on t_a actually reflects the assembly rate of SWNTs. As shown in Figure 12, $R_{t(app)}$, calculated from the slope of the straight line in Figure 11, decreases sharply in the initial assembly stage and then slowly with increasing t_a. The $R_{t(app)}$ value can be used to estimate the surface coverage of SWNTs. For through-bond tunneling across AUT, β is about 1.06/methylene group,[20] d corresponds to 13 methylene groups (11 -CH_2-, 1 -NH-, and 1 C═O). The effective contact resistance R_0 between Au and an individual carbon nanotube is ∼1 GΩ;[28] then R_t for a single SWNT is calculated to be 9.7×10^{14} Ω on the basis of eq 2. Introduction of the R_t and $R_{t(app)}$ values (in Figure 12) into eq 3 yields the surface density of SWNTs. The across section area is $\sim 1.1 \times 10^{-14}$ cm^2 for a single SWNT with a diameter of 1.2 nm. Therefore, the surface coverage of SWNTs can be estimated, which is shown in Figure 7b. The θ_{SWNT} versus t_a plot obtained both in AFM (Figure 7a) and in electrochemical experiments (Figure 7b) demonstrate the same trend: θ_{SWNT} increases sharply in the first 2 h and then slowly with increasing t_a, indicating two distinct assembly kinetics: a relative fast step, which takes ca. 120 min, followed by a slow step, which lasts several hours. As the intensity of G-line (sp^2 C−C stretching mode of SWNTs) in Raman spectrum depends on the density of SWNTs at Au substrates, it can also be employed to investigate the assembly kinetics of SWNTs. Results are shown in Figure 13, from which an initial fast assembly step followed by a slow step can also be observed. This is in good agreement with the results obtained by AFM and electrochemical methods.

The kinetics of the first step is believed to be governed by the surface condensation reaction. In this stage, single SWNTs or SWNT bundles are linked to Au surface separately. When t_a is short, the small width of needlelike domains in AFM images supports this mechanism.[8a,c,10,11a] On the other hand, kinetics of the second step is probably related to the steric hindrance of linked SWNTs to unlinked SWNTs, and the van der Waals interaction in the formation of larger aggregates during the chemical assembly. The increase of the width of needlelike features in AFM images after long modification time gives evidence to this mechanism.[8a,c,10,11a] From Figure 7, it can also be seen clearly that θ values obtained by the electrochemical method are smaller than those obtained by the AFM method. We believe this is due to the following two reasons: (1) AFM tip-induced broadening artifact and (2) some SWNTs, which aggregate side-by-side with SWNTs already immobilized on the gold surface, may not form chemical bonds with the AUT monolayer and then do not contribute to the through-bond tunneling, suggesting that bundle formation rather than surface condensation is dominant during the slow step.

4. Conclusion

SWNTs chemically assembled on AUT monolayer-coated Au substrates show quasireversible CV features, indicating that,

although directly linked to the insulating AUT monolayer, the assembled SWNTs allow electron exchange between gold electrode and the redox couple in solution. We believe electron tunneling between assembled SWNTs and the underlying gold substrate is involved in the charge transfer process. The insulating AUT monolayer between Au substrate and SWNTs acts as an electron tunneling barrier, which leads to interesting dependence of the CV behavior of Au/AUT/SWNT electrode on assembly time. We ascribe the high electron transfer efficiency at Au/AUT/SWNT electrodes to the large p-conjugated system within SWNTs, which enable SWNTs to accept or donate electrons, and to the efficient through-bond tunneling between gold electrode and SWNTs. The apparent tunneling resistance was employed to describe the through-bond tunneling process. The decrease of the apparent tunneling resistance with longer assembly time results in the decrease of peak potential splitting in CV plots, suggesting that apparent tunneling resistance has similar apparent effects to solution resistance. The good agreement between experimental results and theoretical predictions demonstrates that the theory of solution resistance can be successfully used to describe the apparent tunneling resistance. Kinetic studies with AFM, electrochemistry, and Raman spectroscopy have shown two distinct assembly kinetics with the initial fast step taking ca. 2 h and the second slow step lasting several hours. Moreover, we believe the fast step is dominated by the surface reaction and the successive slow step is governed by bundle formation.

Acknowledgment. Financial support from the National Natural Science Foundation of China (NSFC, 20373005) and the Ministry of Science and Technology (MOST, 2001CB6105) is gratefully acknowledged.

References and Notes

(1) (a) Iijima, S.; Ichihashi, T. *Nature* **1993**, *363*, 603. (b) Bethune, D. S.; Kiang, C. H.; de Vries, M. S.; Gorman, G.; Savoy, R.; Vasquez, J.; Beyers, R. *Nature* **1993**, *363*, 605.

(2) (a) Trans, S. J.; Devoret, M. H.; Dai, H. J.; Thess, A.; Smalley, R. E., Geerligs; Dekker, C. *Nature* **1997**, *386*, 474. (b) Bockrath, M.; Cobden, D. H.; McEuen, P. L.; Chopra, N. G.; Zettle, A. *Science* **1997**, *275*, 1922. (c) Trans, S. J.; Verschueren, A. R. M.; Dekker, C. *Nature* **1998**, *393*, 49. (d) Martel, R.; Schmidt, T.; Shea, H. R.; Hertel, T.; Avouris, Ph. *Appl. Phys. Lett*. **1998**, *73*, 2447. (e) Collins, P. G.; Zettle, A.; Bando, H.; Thess, A.; Smalley, R. E. *Science* **1997**, *278*, 100. (f) Antonov, R.; Johnson, A. T. *Phys. Rev. Lett*. **1999**, *83*, 3274. (g) Fuhrer, M. S.; Nygard, J.; Shih, L.; Forero, M.; Yoon, Y. G.; Mazzoni, M. S. C.; Choi, H. J.; Ihm, J.; Louie, S. G.; Zettle, A.; McEuen, P. L. *Science* **2000**, *288*, 494.

(3) (a) de Heer, W. A.; Chatelain, A.; Ugarte, D. *Science* **1995**, *270*, 1179. (b) Fan, S. S.; Chapline, M. G.; Franklin, N. R.; Tombler, T. W.; Cassell, A. M.; Dai, H. J. *Science* **1999**, *283*, 512.

(4) (a) Wong, S. S.; Joselevich, E.; Woolley, A. T.; Cheung, C. L.; Lieber, C. M. *Nature* **1998**, *394*, 52. (b) Wong, S. S.; Harper, J. D.; Lansbury, P. T.; Lieber, C. M. *J. Am. Chem. Soc.* **1998**, *120*, 603. (c) Wong, S. S.; Woolley, A. T.; Joselevich, E.; Cheung, C. L.; Lieber, C. M. *J. Am. Chem. Soc.* **1998**, *120*, 8557.

(5) Baughman, R. H.; Cui, C. X.; Zakhidov, A. A.; Lqbal, Z.; Barisci, J. N.; Spinks, G. M.; Wallace, G. G.; Mazzoldi, A.; De Rossi, D.; Rinzler, A. G.; Jaschinski, O.; Roth, S.; Kertesz, M. *Science* **1999**, *284*, 1340.

(6) (a) Kong, J.; Franklin, N. R.; Zhou, C.; Chapline, M. G.; Peng, S.; Cho, K.; Dai, H. J. *Science* **2000**, *287*, 622. (b) Collins, P. G.; Bradley, K.; Ishigami, M.; Zettle, A. *Science* **2000**, *287*, 1801.

(7) (a) Li, W. Z.; Xie, S. S.; Qian, L. X.; Chang, B. H.; Zou, B. S.; Zhou, W. Y.; Zhao, R. A.; Wang, G. *Science* **1996**, *274*, 1701. (b) Ren, Z. F.; Huang, Z. P.; Xu, J. W.; Wang, J. H.; Bush, P.; Siegal, M. P.; Provencio, P. N. *Science* **1998**, *282*, 1105. (c) Huang, S.; Dai, L.; Mau, A. W. H. *J. Phys. Chem. B* **1999**, *103*, 4223. (d) Choi, Y. C.; Shin, Y. M.; Lee, Y, H.; Lee, B. S.; Park, G. S.; Choi, W. B.; Lee, N. S.; Kim, J. M. *Appl. Phys. Lett*. **2000**, *76*, 2367.

(8) (a) Liu, Z. F.; Shen, Z. Y.; Zhu, T.; Huo, S. F.; Ying, L. Z.; Shi, Z. J.; Gu, Z. N. *Langmuir* **2000**, *16*, 3569. (b) Wu, B.; Zhang, J.; Wei Z.; Cai, S. M.; Liu, Z. F. *J. Phys. Chem. B* **2001**, *105*, 5075. (c) Diao, P.; Liu, Z. F.; Wu, B.; Nan, X. L.; Zhang, J.; Wei, Z. *ChemPhysChem*. **2002**, *3*, 898. (d) Yang, Y. L.; Zhang, J.; Nan, X. L.; Liu, Z. F. *J. Phys. Chem. B* **2002**, *106*, 4139. (e) Peng, H. L.; Chen, Z.; Tong, L. M.; Yu, X. C.; Ran, C. B.; Liu, Z. F. *J. Phys. Chem. B* **2005**, *109*, 3526. (f) Chen, Z.; Yang, Y. L.; Wu, Z. Y.; Luo, G.; Xie, L. M.; Liu, Z. F.; Ma, S. J.; Guo, W. L. *J. Phys. Chem. B* **2005**, *109*, 5473.

(9) Chattopadhyay, D.; Galeska, I.; Papadimitrakopoulos, F. *J. Am. Chem. Soc.* **2001**, *123*, 9451.

(10) Gooding, J. J.; Wibowo, R.; Liu, J.; Yang, W.; Losic, D.; Orbons, S.; Mearns, F. J.; Shapter, J. G.; Hibbert, D. B. *J. Am. Chem. Soc.* **2003**, *125*, 9006.

(11) (a) Patolsky, F.; Weizmann, Y.; Willner, I. *Angew. Chem., Int. Ed*. **2004**, *43*, 2113. (b) Sheeney-Haj-Ichia, L.; Basner, B.; Willner, I. *Angew. Chem., Int. Ed.* **2005**, *44*, 78.

(12) Cassell, A. M.; Raymakers, J. A.; Kong, J.; Dai, H. *J. Phys. Chem. B* **1999**, *103*, 6484.

(13) Chen, J.; Hamon, M. A.; Hu, H.; Chen, Y.; Rao, A. M.; Eklund, P. C.; Haddon, R. C. *Science* **1998**, *282*, 95.

(14) (a) Freeman R. G.; Grabar, K. C.; Allison, K. J.; Bright, R. M.; Davis, A. J.; Guthrie A. P.; Hommer, M. B.; Jackson, M. A.; Smith, P. C.; Walter, D. G.; Natan, M. J. *Science* **1995**, *267*, 1629. (b) Bharathi, S.; Nogami, M.; Ikeda, S. *Langmuir* **2001**, *17*, 1.

(15) (a) Amatore, C.; Saveant, J. M.; Tessier, D. *J. Electroanal. Chem.* **1983**, *147*, 39. (b) Diao, P.; Guo, M.; Tong, R. T. *J. Electroanal. Chem.* **2001**, *495*, 98.

(16) Bard, A. J.; Faulkner, L. R. *Electrochemical Methods*; John Wiley & Sons: New York, 1980; p 129.

(17) Campbell, J. K.; Sun, L.; Crooks, R. M. *J. Am. Chem. Soc.* **1999**, *121*, 3779.

(18) McCreery, R. L. In *Electroanalytical Chemistry*; Bard, A. J., Ed.; Dekker: New York, 1991; Vol. 17, pp 221−374.

(19) (a) Porter, M. D.; Bright, T. B.; Allara, D. L.; Chidsey, C. E. D. *J. Am. Chem. Soc*. **1987**, *109*, 3559. (b) Diao, P.; Jiang, D. L.; Cui, X. L.; Gu, D. P.; Tong, R. T.; Zhong, B. *J. Electroanal. Chem.* **1999**, *464*, 61.

(20) Finklea, H. O.; Hanshew, D. D. *J. Am. Chem. Soc.* **1992**, *114*, 3174.

(21) Chidsey, C. E. D.; Bertozzi, C. R.; Putvinski, T. M.; Mujsce, A. M. *J. Am. Chem. Soc.* **1990**, *112*, 4301.

(22) Chidsey, C. E. D. *Science* **1991**, *251*, 919.

(23) Bain, C. D.; Troughton, E. B.; Tao, Y. T.; Evall, J.; Whitesides, G. M.; Nuzzo, R. G. *J. Am. Chem. Soc.*, **1989**, *111*, 321.

(24) Cui, X. D.; Primak, A.; Zarate, X.; Tomfohr, J.; Sankey, O. F.; Moore, A. L.; Moore, T. A.; Gust, D.; Harris, G.; Lindsay, S. M. *Science* **2001**, *294*, 571.

(25) Cui, X. D.; Primak, A.; Zarate, X.; Tomfohr, J.; Sankey, O. F.; Moore, A. L.; Moore, T. A.; Gust, D.; Nagahara, L. A.; Lindsay, S. M. *J. Phys. Chem. B* **2002**, *106*, 8609.

(26) (a) Engelkes, V. B.; Beebe, J. M.; Frisbie, C. D. *J. Am. Chem. Soc.* **2004**, *126*, 14287. (b) Beebe, J. M.; Engelkes, V. B.; Miller, L. L.; Frisbie, C. D. *J. Am. Chem. Soc.* **2002**, *124*, 11268.

(27) Nicholson, R. S. *Anal. Chem.* **1965**, *37*, 1351.

(28) Bachtold, A.; Henny, M.; Terrier, C.; Strunk, C.; Schõnenberger, C.; Salvetat, J. P.; Bonard, J. M.; Forro, L. *Appl. Phys. Lett.* **1998**, *73*, 274.